diabetes®
American Diabetes Association®

Metrnl Alleviates Lipid Accumulation by Modulating Mitochondrial Homeostasis in Diabetic Nephropathy

Yuxia Zhou, Lu Liu, Bangming Jin, Yixuan Wu, Lifen Xu, Xuebing Chang, Laying Hu, Guifang Wang, Yali Huang, Lingyu Song, Tian Zhang, Yuanyuan Wang, Ying Xiao, Fan Zhang, Mingjun Shi, Lingling Liu, Tuanlao Wang, Rui Yan, and Bing Guo

Diabetes 2023;72(5):611–626 | https://doi.org/10.2337/db22-0680

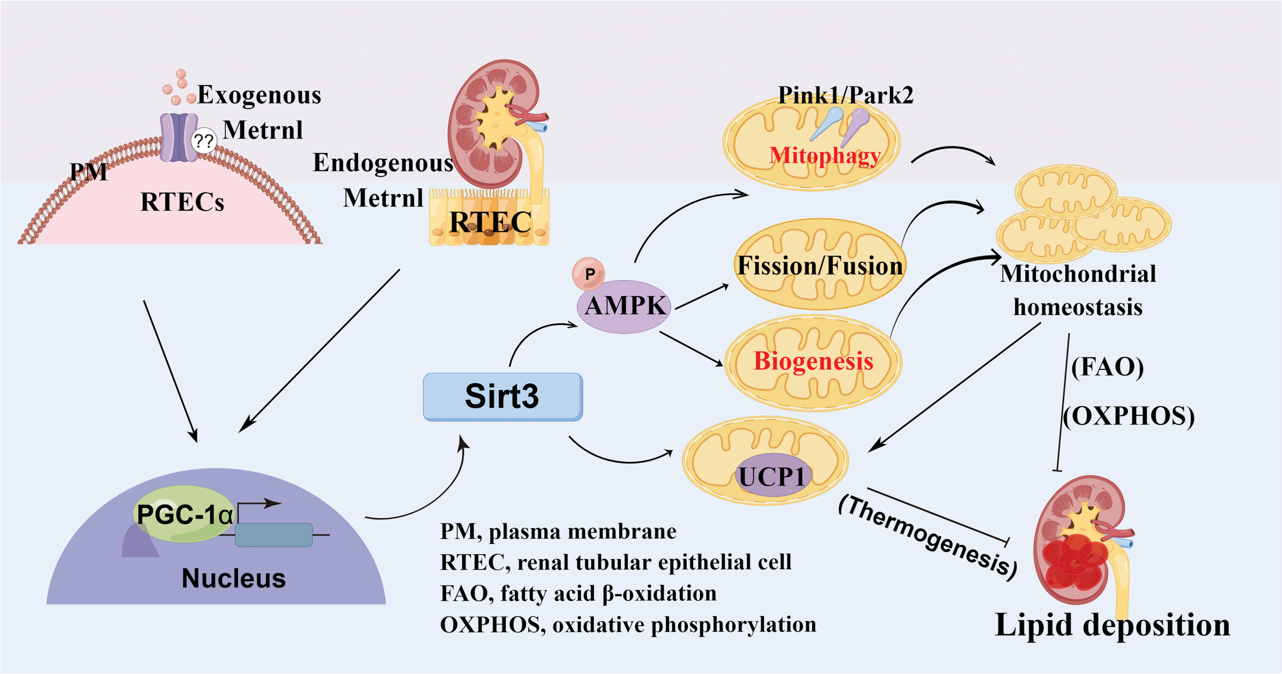

Metrnl Alleviates Lipid Accumulation by Modulating Mitochondrial Homeostasis in Diabetic Nephropathy

Yuxia Zhou,[1,2,3,4] Lu Liu,[4] Bangming Jin,[2,3,5] Yixuan Wu,[4] Lifen Xu,[4] Xuebing Chang,[4] Laying Hu,[4] Guifang Wang,[4] Yali Huang,[4] Lingyu Song,[4] Tian Zhang,[2,3,4] Yuanyuan Wang,[2,3,4] Ying Xiao,[2,3,4] Fan Zhang,[2,3,4] Mingjun Shi,[2,3,4] Lingling Liu,[2,3,4] Tuanlao Wang,[6] Rui Yan,[1] and Bing Guo[2,3,4]

Diabetes 2023;72:611–626 | https://doi.org/10.2337/db22-0680

Ectopic lipid accumulation in renal tubules is closely related to the pathogenesis of diabetic kidney disease (DKD), and mitochondrial dysfunction is thought to play a key role in lipid accumulation. Therefore, maintaining mitochondrial homeostasis holds considerable promise as a therapeutic strategy for the treatment of DKD. Here, we report that the Meteorin-like (Metrnl) gene product mediates lipid accumulation in the kidney and has therapeutic potential for DKD. We confirmed the reduced expression of Metrnl in renal tubules, which was inversely correlated with DKD pathological changes in human patients and mouse models. Functionally, pharmacological administration of recombinant Metrnl (rMetrnl) or Metrnl overexpression could alleviate lipid accumulation and inhibit kidney failure. In vitro, rMetrnl or Metrnl overexpression attenuated palmitic acid–induced mitochondrial dysfunction and lipid accumulation in renal tubules accompanied by maintained mitochondrial homeostasis and enhanced lipid consumption. Conversely, shRNA-mediated Metrnl knockdown diminished the protective effect on the kidney. Mechanistically, these beneficial effects of Metrnl were mediated by the Sirt3-AMPK signaling axis to maintain mitochondrial homeostasis and through Sirt3-uncoupling protein-1 to promote thermogenesis, consequently alleviating lipid accumulation. In conclusion, our study demonstrates that Metrnl regulated lipid metabolism in the kidney by modulating mitochondrial function and is a stress-responsive regulator of kidney pathophysiology, which sheds light on novel strategies for treating DKD and associated kidney diseases.

ARTICLE HIGHLIGHTS

- Metrnl is expressed in renal tubules and is reduced under diabetic conditions.
- The concentration of Metrnl in the kidney is correlated with lipid accumulation and serum creatinine.
- Metrnl-specific overexpression in the kidney or recombinant Metrnl administration alleviates renal injuries in diabetic mice.
- Metrnl regulates renal tubules lipid metabolism through Sirt3-AMPK/UCP1 signaling axis–mediated mitochondrial homeostasis.

Patients with diabetic kidney disease (DKD) often have lipid metabolism disorders, and dyslipidemia occurs during all stages of the disease (1). Ectopic lipid deposition refers to excessive accumulation of lipids, especially triglycerides (TGs), in nonadipose tissues, such as kidney, liver, heart, and pancreas (2,3), causing lipotoxic damage and resulting in a series of pathophysiological changes. Incomplete fatty acid oxidation (FAO) and lipid peroxidation cause oxidative stress, endoplasmic reticulum stress, and

---

[1]Department of Nephrology, Affiliated Hospital of Guizhou Medical University, Guiyang, China
[2]International Scientific and Technological Cooperation Base of Pathogenesis and Drug Research on Common Major Diseases, Guizhou Medical University, Guiyang, China
[3]Guizhou Provincial Key Laboratory of Pathogenesis and Drug Research on Common Chronic Diseases, Guizhou Medical University, Guiyang, China
[4]Department of Pathophysiology, Guizhou Medical University, Guiyang, China
[5]Department of Physiology, Guizhou Medical University, Guiyang, China
[6]School of Pharmaceutical Sciences, State Key Laboratory of Cellular Stress Biology, Fujian Provincial Key Laboratory of Innovative Drug Target Research, Xiamen University, Fujian, China

Corresponding author: Bing Guo, guobingbs@126.com, or Tuanlao Wang, xmuibrwtl@xmu.edu.cn, or Rui Yan, yryr1234@126.com

Received 9 August 2022 and accepted 15 February 2023

This article contains supplementary material online at https://doi.org/10.2337/figshare.22120454.

Y.Z., Lu Liu, and B.J. contributed equally to this work.

activation of proinflammatory processes (4,5). Recent evidence indicates that during DKD, lipid accumulation occurs in podocytes, mesangial cells, and proximal tubular epithelial cells (6–8). The proximal tubules have a high energy demand; they have relatively little glycolytic capacity and rely on mitochondrial β-oxidation of free fatty acids to maximize ATP production (4,9). Mitochondrial integrity is necessary for proper oxidative phosphorylation and ATP production (10,11). Abnormalities in mitochondria in proximal tubules have been found in patients with DKD and in mouse models (12–14). Therefore, it is important to identify new therapeutic and preventive strategies to support proximal tubule mitochondrial function and alleviate ectopic lipid deposition by exploiting key components in a network of cellular processes.

Meteorin-like (Metrnl) is a recently identified hormone that is produced by skeletal muscle and adipose tissue in response to exercise and cold exposure, respectively (15,16), and exerts metabolic effects that improve glucose metabolism and diabetes (17–19). Recently, it has been shown that serum Metrnl concentrations are inversely correlated with renal function and DKD (20). However, to our knowledge, the role played by Metrnl in the kidney has not been explored. The observation of Metrnl expression in the kidney prompted us to examine the role of Metrnl in the kidney.

In this study, we identified a cytokine, Metrnl, whose function has not been reported in the kidney, to our knowledge, as a potentially important regulator of kidney metabolism to maintain cellular mitochondrial homeostasis and lipid accumulation in DKD via Metrnl–Sirt3–AMPK/UCP1 signaling in renal tubular epithelial cells (RTECs). Moreover, we found that Metrnl expression was remarkably reduced in the kidney of patients with DKD and mice. Importantly, pharmacological administration of recombinant Metrnl (rMetrnl) or Metrnl overexpression effectively alleviated lipid accumulation and kidney failure, suggesting that Metrnl may be an attractive therapeutic candidate for DKD.

RESEARCH DESIGN AND METHODS

Human Renal Biopsy Samples

Characteristics of renal biopsy samples are described in Supplementary Table 1. Our investigations were conducted in accordance with the principles of the Declaration of Helsinki and were approved by the Research Ethics Committee of Guizhou Medical University.

Animal Studies

All animal experiments were performed according to guidelines for the care of laboratory animals in strict compliance with the regulations of the Guizhou Medical University Institutional Animal Ethics Committee.

Establishment of High-Fat Diet– and Streptozotocin-Induced Diabetic Mice and a *db/db* Mouse Model

Male C57BL/6 mice, 8 weeks old, were fed high-fat diets (HFDs) (Dyets) for 4 months to induce obesity and insulin resistance. Then, streptozotocin (STZ) 55 mg/kg body weight was administered intraperitoneally to the mice daily for 3 days, and HFD diets or control diets (NCDs) were maintained for another 3 months.

Male wild-type mice and *db/db* mice, 10 weeks old (GemPharmatech), were fed normal diets for another 30 weeks. The physical and biochemical parameters of experimental animals are listed in Supplementary Table 2.

rMetrnl Protein Intervention in Diabetic Mice

Endotoxin-free rMetrnl for mice (AtaGenix) was administrated at a dose of 0.3 mg/kg body weight to *db/db* mice by tail vein injection every other day for 8 weeks beginning at age 12 weeks; saline (vehicle) was the control. After 8 weeks of administration, all mice were then maintained on the same diets for another 8 weeks.

Metrnl Overexpression Intervention in Diabetic Mice

Adeno-associated virus–9 expressing Metrnl (AAV9-Metrnl) and control virus (AAV9-vector) were administered to *db/db* mice via a tail-vein injection apparatus (Yiyan), and 100 μL of AAV9-Metrnl or AAV9-vector (1×10^{11} pfu/mL) was aspirated once with a 29G insulin syringe. To cause Metrnl-specific overexpression in kidney through intrarenal pelvic injection of AAV9-Metrnl into *db/db* mice, the mice were anesthetized with isoflurane, the kidney was leaked by dissecting the back, and then the adeno-associated virus was injected into the kidney through the renal pelvis.

Cell Culture and Treatments

Rat proximal tubule epithelial cells, NRK-52E, were obtained from ATCC and cultured in DMEM (1.0 g/L glucose) containing 10% FBS. rMetrnl was added to the medium at a final concentration of 200 ng/mL and cells were exposed to 0.25 mmol/L palmitic acid (PA) for 48 h. We obtained 293T cell lines from ATCC and cultured them in DMEM (4.5 g/L glucose) containing 10% FBS.

Histological Analysis of Renal Tissues

Hematoxylin and eosin (H-E) staining and immunohistochemistry (IHC) analysis were performed as described in our previous study (21). Periodic acid Schiff (PAS) staining was performed using a staining kit according to the manufacturer's instructions (Solarbio). Tissue sections were photographed with an Olympus BX53 microscope. The staining was quantified in positive areas using ImageJ Pro Plus 6.0 software (U.S. National Institutes of Health).

RNA Isolation and RT-qPCR

RNA of tissues or cells was extracted with TRIzol reagent, and then reverse transcribed into cDNA using the PrimeScriptRT Master Mix. RT-qPCR was performed using SYBR Green Master Mix. Fold change in gene expression normalized to GAPDH was calculated by the comparative cycle threshold method. The primers used in this study are listed in Supplementary Table 3.

Western Blot Analysis

Tissues or cell pellets were resuspended in Lysis Buffer containing a protease inhibitor cocktail of phenylmethylsulfonyl fluoride and phosphatase inhibitor. Approximately 10–100 μg of soluble supernatant of tissue lysates or proteins from cell lysates were separated by SDS-PAGE. The selected proteins were probed with the antibodies listed in Supplementary Table 4.

Immunofluorescence Technique

Immunofluorescence staining was performed as described previously (22). In brief, cell coverslips or tissue sections (3 μm) were incubated with different primary antibodies and subsequently incubated with secondary Alexa 488 or 555 conjugated antibody. The images were obtained by a FV3000 laser-scanning confocal microscope system (Olympus).

Oil Red O Staining and Nile Red Staining

Frozen sections (8 μm) or cell coverslips were fixed in 4% paraformaldehyde and stained with 0.3% Oil Red O dye solution dissolved in 60% isopropanol for 10 min, after washing with PBS. They subsequently were counterstained with hematoxylin and mounted with 50% glycerin. For Nile Red staining, sections were stained with 0.01 mg/mL Nile red solution for 1 h to visualize lipid droplets.

Lentivirus-Mediated Gene Expression and Interference

Metrnl or Sirt3 overexpression was achieved by a pCDH-CMV-MCS-EF1-Puro vector (OE-Metrnl or OE-Sirt3). The silencing of the UCP1 or Metrnl gene was performed using a pLK0.1-TRC-copGFP-Puro vector (sh-UCP1 or sh-Metrnl), both mediated by a lentivirus expression system. The sequences of shRNA oligonucleotides are listed in Supplementary Table 3. A nicotinamide analog, 3-TYP, was used as a Sirt3 inhibitor.

Spatial Transcriptomic Analysis

Spatial transcriptomic analysis was performed as described (23). Briefly, samples were collected and embedded in optimal cutting temperature compound then cryo-sectioned and stained with 1% cresyl violet. Cells of interest were harvested by Cellcut Plus laser capture microdissection (LCM) (MMI). Cells obtained were lysed for the first cDNA synthesis, and a modified Smart2-sequencing protocol was performed to amplify the cDNA. Next-generation sequencing was conducted by the Haplox Genomics Center with Illumina NovaSeq6000.

Lipid Sample Preparation and Lipidomic Assay

Renal cortical tissues (50 mg) were subjected to liquid extraction. For untargeted lipidomics analysis, lipid extraction and mass spectrometry-based lipid detection were performed by Applied Protein Technology (Shanghai).

RNA-Sequencing Analysis

The library construction and sequencing were performed at Beijing Novogene. The enrichment analysis was analyzed with Kyoto Encyclopedia of Genes and Genomes (KEGG) database (https://www.kegg.jp/) and gene ontology (GO) annotation was performed with DAVID (https://david.ncifcrf.gov/tools.jsp). Genes were considered significantly differentially expressed if the adjusted *P* value was <0.05 as determined by DESeq2.

MitoTracker Red CMXRos Assay and Mitochondrial Membrane Potential Assay

MitoTracker Red CMXRos assay was detected by a kit from Cell Signaling Technology. Mitochondrial membrane potential was detected using the JC-1 assay kit (Beyotime).

Seahorse Analysis

The Seahorse XF Extracellular Flux Bioanalyzer (Agilent) was used to measure oxygen consumption rate (OCR). The level of oxygen consumption was detected using a XFp Cell Mito Stress Test Kit (Agilent) according to the manufacturer's instructions.

mtDNA

The relative copy number of mtDNA was detected by RT-qPCR assay. Total DNA was extracted with a genomic DNA kit. mtDNA was amplified using primers for the mitochondrial cytochrome c oxidase subunit 2 (COX2) gene and β-actin for nuclear DNA. The ratio of mtDNA to β-actin was calculated and served as the mtDNA copy number. The primers are listed in Supplementary Table 3.

Chromatin Immunoprecipitation Assay

A chromatin immunoprecipitation (ChIP) assay was performed using a kit from Cell Signaling Technology. In brief, DNA–protein complexes were cross-linked using 1% formaldehyde for 15 min. The cross-linked chromatin samples were isolated by nuclease digestion. PGC-1α was immunoprecipitated using a PGC-1α or IgG antibody, and then DNA was extracted. For qPCR, ChIP DNA was amplified using primers of Sirt3 promoter (Supplementary Table 3) by RT-qPCR. Values represent the percentage of input using the comparative cycle threshold method.

Statistical Analysis

Statistical significance between two groups was assessed using Student *t* tests or among multiple groups using two-way ANOVA.

Data and Resource Availability

Data and resources are available from the corresponding authors.

RESULTS

Reduced Expression of Metrnl in the Kidneys of Diabetic Mice and of Patients With DKD

Metrnl was ubiquitously expressed in multiple adult tissues, including the heart, liver, kidney, and pancreas (Supplementary Fig. 1*A*). Furthermore, according to The Human

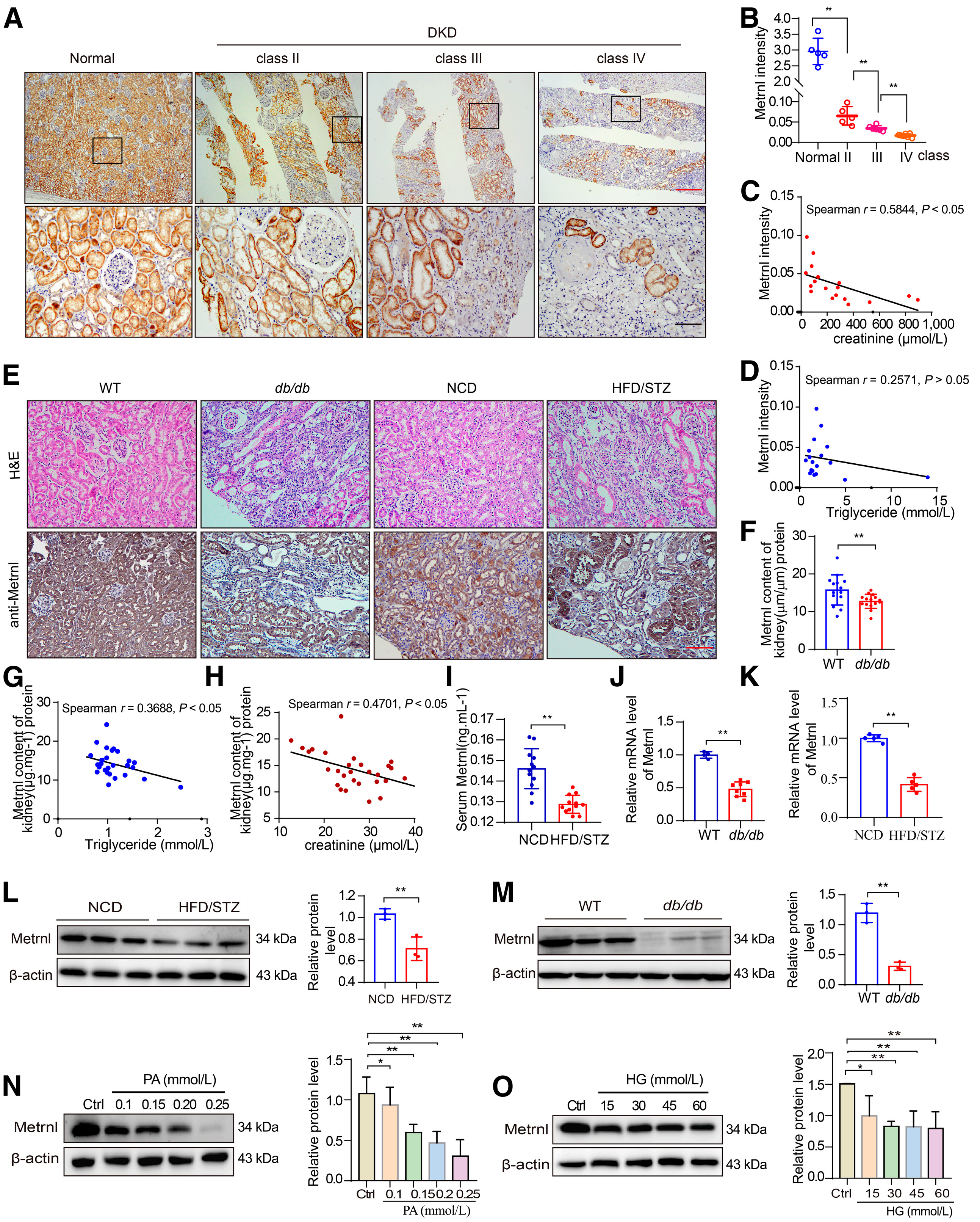

Figure 1—Reduced expression of Metrnl in the kidneys of diabetic mice and of patients with DKD. *A* and *B*: Representative IHC images (*A*) and quantification (*B*) of Metrnl expression in human renal cortical tissues from normal kidney poles ($n = 5$) and patients with mild (class II; $n = 5$), moderate (class III; $n = 6$), or severe (class IV; $n = 7$) histopathological lesions of DKD. Scale bars: red, 500 μm; black, 100 μm. *C* and *D*: Correlation between Metrnl expression in human renal cortical tissues from patients with DKD and Scr ($n = 18$) (*C*) or serum TG ($n = 18$) (*D*) in all patients. *E*: Representative H-E and IHC images indicating Metrnl protein expression of kidney in 40-week-old *db/db* mice and STZ/HFD-induced diabetic mice. Scale bar: 100 μm. *F*: The protein level of Metrnl measured by ELISA in the renal cortex from

Protein Atlas database (https://www.proteinatlas.org), Metrnl is highly expressed in renal tubules. Considering the specific expression of Metrnl in the kidney, we examined the role played by Metrnl in DKD. IHC staining showed that the level of Metrnl was obviously reduced in renal biopsy specimens from patients with DKD. Moreover, Metrnl was mainly expressed in renal tubules and gradually decreased with the progression of DKD (Fig. 1*A* and *B*). Notably, the level of Metrnl in renal tubules was negatively correlated with serum creatinine (Scr) levels (Fig. 1*C*). There was a negative correlation, although not a significant one, between serum TG levels and Metrnl expression (Fig. 1*D*). In addition, serum levels of Metrnl were lower in diabetic mice than in control mice (Fig. 1*I*). IHC staining and Western blot analysis revealed reduced Metrnl expression in damaged renal tubules and in the kidneys of STZ/HFD-induced diabetic mice and *db/db* mice (Fig. 1*E*, *L*, and *M*). Reduced Metrnl mRNA levels were observed in the kidneys of the STZ/HFD-induced mice and *db/db* mice (Fig. 1*J* and *K*), and also in the proximal renal tubules of *db/db* mice, as captured by LCM (Fig. 2*D*). Similarly, a negative correlation between the protein levels of Metrnl in the renal cortex and the levels of serum TGs, as well as of Scr, was observed in all *db/db* diabetic mice (Fig. 1*F*–*H*).

Because Metrnl was mainly located in the renal tubules, the function of Metrnl was further examined in RTECs. In vitro, the protein level of Metrnl was significantly dose-dependently reduced in RTECs treated with high glucose or PA (Fig. 1*N* and *O*). These results suggest the reduction in Metrnl is closely associated with diabetic kidney pathophysiology.

Lipid Deposition and Mitochondrial Dysfunction Are Positively Correlated With DKD

To fully understand the mechanism of renal tubule injury in diabetes, we used LCM technology to dissect a number of renal tubule cells in situ to specifically harvest cells of interest and obtain cells with known spatial information. The proximal renal tubules of 40-week-old *db/db* mice were captured by LCM (Fig. 2*A*), and the RNA was subjected to smart RNA sequencing. Enrichment analysis of KEGG-related pathways showed that differentially abundant components correlated with oxidative phosphorylation (OXPHOS), thermogenesis, and autophagy pathways (Fig. 2*B* and *C*, Supplementary Fig. 2*A*). Genes related to the pathways were further examined by qPCR (Fig. 2*D*), and the results showed that the expression of genes related to lipogenesis (namely, Scd1) was increased, whereas expression of genes related to fatty acid β-oxidation (namely, PGC-1α, Cpt1α), OXPHOS (Atp5b, Ndufa10), and mitophagy/autophagy (Rab7, PTEN-induced putative kinase 1 [Pink1], and Atg7) was downregulated in the proximal renal tubules, suggesting that defects in mitochondrial function may be an important cause of renal tubule injury in diabetic mice.

Interestingly, results of Oil Red O or Nile red staining of tissues from the HFD/STZ-induced diabetic nephropathy mouse model showed plentiful lipid deposition in the kidney tissue of mice, especially in the renal tubules (Fig. 2*E* and *F*). The protein expression of perilipin-2, a lipid droplet–coating protein, was significantly elevated, as determined by immunofluorescence analysis and Western blotting (Fig. 2*G* and *H*; Supplementary Fig. 2*B* and *C*). Similar results were observed in renal biopsy samples from patients with DKD; perilipin-2 expression was significantly increased in remnant renal tubules, and immunofluorescence and IHC analysis showed lipid deposition gradually increased with disease progression (Fig. 2*I*–*K*). These findings demonstrated that lipid deposition and mitochondrial dysfunction were positively correlated with pathophysiological alternation in DKD.

Metrnl Negatively Regulates Lipid Accumulation in the Kidneys of Mice With DKD

Here, we observed that Metrnl expression in RTECs was greatly downregulated by PA stimulation compared with high-glucose stimulation. Moreover, the protein level of Metrnl in renal tubules (Fig. 1*B*) was negatively correlated with perilipin-2 expression (Fig. 2*K*) in renal biopsy samples from patients with DKD, as measured by correlation analysis (Supplementary Fig. 3*A*), suggesting that Metrnl may play an important role in lipid metabolism. To examine the effect of Metrnl on lipotoxicity under PA stimulation, we constructed lentivirus-mediated stable cell lines with Metrnl overexpression and knockdown (Supplementary Fig. 3*B* and *C*) and found that silencing Metrnl resulted in lipid accumulation, as confirmed by increased levels of Oil Red O staining in PA-treated RTECs (Fig. 3*A*). Conversely, Metrnl overexpression significantly reduced lipid accumulation (Fig. 3*B*). Moreover, Oil Red O staining showed the reduced lipid deposition in the kidneys of *db/db* mice, which were administered rMetrnl (Fig. 3*C*), and further experiments confirmed that lipid deposition was reduced in mice overexpressing AAV9-Metrnl (Supplementary Fig. 3*D*). Reduced expression of perilipin-2 was also observed at the protein level in *db/db* mice overexpressing Metrnl and those treated with rMetrnl (Fig. 3*D* and *E*). In vitro, Metrnl overexpression or exposure to exogenous rMetrnl significantly inhibited perilipin-2 expression in PA-treated RTECs compared with the control (Fig. 3*F* and *G*),

db/db diabetic mice (wild type [WT], *n* = 14; *db/db*, *n* = 15). *F*–*H*: Correlation between Metrnl expression (*F*) and serum TG (*G*) or Scr (*H*) in *db/db* diabetic mice (WT, *n* = 14; *db/db*, *n* = 15). *I*: The serum level of Metrnl measured by ELISA in STZ/HFD-induced diabetic mice (*n* = 12) and NCD-fed mice (*n* = 12). *J* and *K*: qPCR analysis of Metrnl mRNA levels in the renal cortex of *db/db* diabetic mice (WT, *n* = 4; *db/db*, *n* = 8) (*J*) and STZ/HFD-induced diabetic mice (NCD, *n* = 5; STZ/HFD, *n* = 5) (*K*). *L* and *M*: Representative Western blot and quantification of Metrnl expression in the kidney from STZ/HFD-induced diabetic mice (*L*) and 40-week-old *db/db* mice (*M*), compared with NCD-fed mice and WT mice, respectively. *N* and *O*: Representative Western blot and quantification of Metrnl expression in NRK-52E cells exposed to PA (0.1, 0.15, 0.2, and 0.25 mmol/L) (*N*) or high concentration of glucose (HG) (15, 30, 45, and 60 mmol/L) (*O*) for 48 h. Data are reported as mean ± SD. $*P < 0.05$, $**P < 0.01$. Ctrl, control.

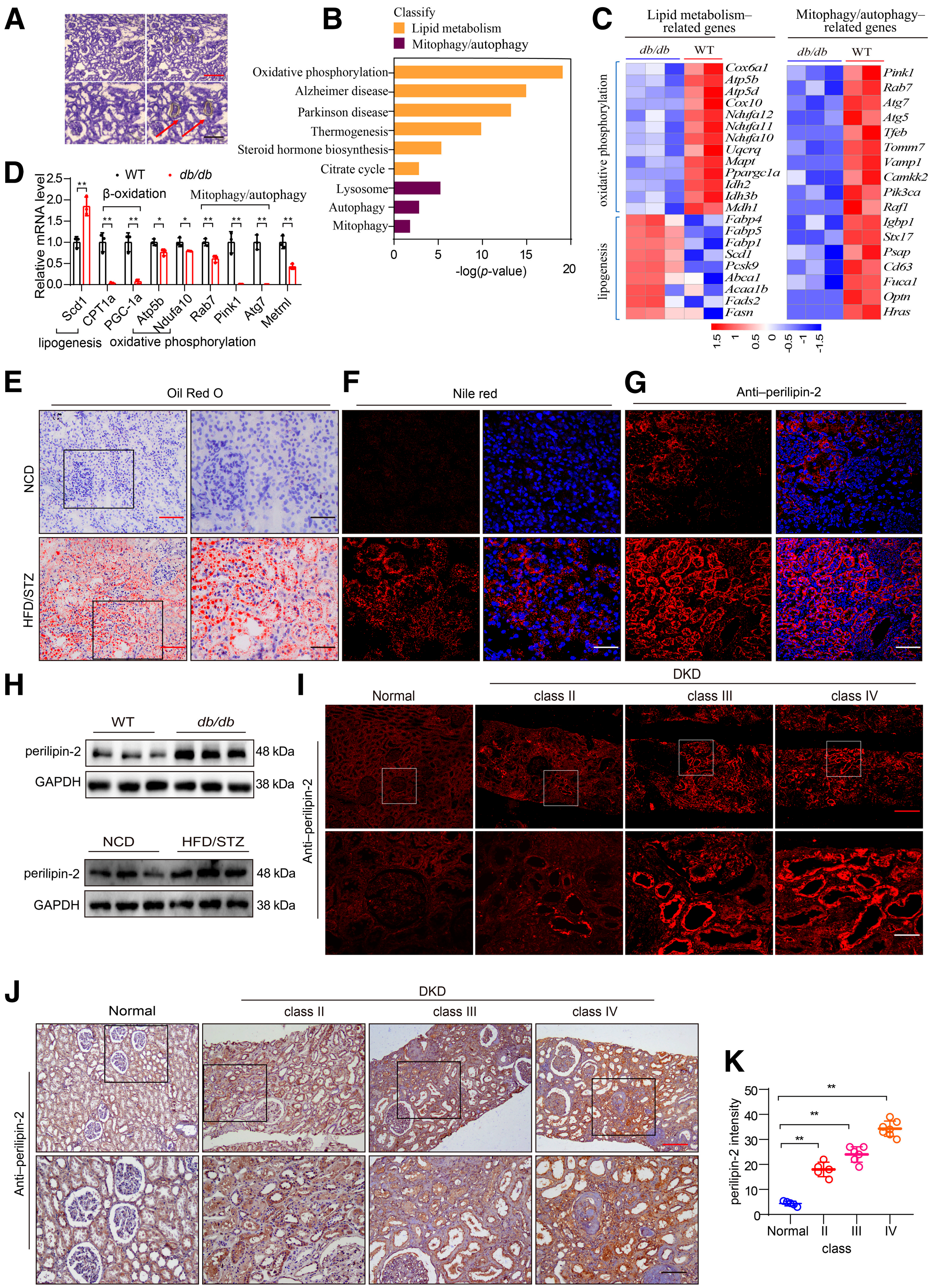

Figure 2—Lipid deposition and mitochondrial dysfunction are positively correlated with DKD. *A*: Kidney sections were stained with 1% (wt/vol) cresyl violet and then subjected to LCM to dissect a number of proximal renal tubules from 40-week-old *db/db* mice. Scale bars: red, 60 μm; black, 30 μm. *B*: Pathway enrichment analysis related to lipid metabolism and mitophagy/autophagy in proximal renal tubules of *db/db* mice based on RNA-sequencing data (wild type [WT], *n* = 2; *db/db*, *n* = 3). *C*: Heat map of the representative, differentially expressed genes related to lipid metabolism (left) and mitophagy/autophagy (right) in the indicated groups based on RNA-sequencing data (WT, *n* = 2; *db/db*, *n* = 3). *D*: Changes in relative mRNA levels of genes related to lipogenesis (Scd1), fatty acid β-oxidation (PGC-1α,

whereas Metrnl knockdown enhanced the expression of perilipin-2 (Fig. 3*H*).

The beneficial effect of rMetrnl on DKD mice was verified by quantifying lipid species by liquid chromatography–mass spectrometry–based lipidomics analysis, and we observed changes in different kinds of lipids, such as sphingomyelin (SM), phosphatidylethanolamine (PE), diglyceride (DG), and cardiolipin (CL) (Fig. 3*I–L*). Notably, the results showed that levels of CL, a phospholipid that is uniquely distributed in the inner mitochondrial membrane (24,25) and participates in OXPHOS and ATP synthesis, were significantly increased after rMetrnl treatment. PE is the second most abundant mitochondrial phospholipid, and it can modulate ATP production (24,26). Some species of PE were also increased after rMetrnl treatment. SM is one of the major phospholipids in membrane microdomains and plays a key role in lipid uptake and glucose homeostasis (24). The accumulation of SM in the renal cortex inhibits AMPK activity and contributes to lipid deposition (27). We found that SM and DG levels in the renal cortex were significantly reduced after rMetrnl treatment. In addition, TG levels were also dramatically reduced in the kidney of rMetrnl-treated *db/db* mice (Supplementary Fig. 3*E*). These results suggest that rMetrnl treatment may modulate CL and SM levels, which are responsible for maintaining of mitochondrial membrane homeostasis against diabetes and reducing lipid deposition.

Changes in Metrnl Expression Are Associated With Changes in Mitochondrial Homeostasis

On the basis of the observation that Metrnl is closely related to lipid accumulation during DKD progression, we examined the mechanism of lipid accumulation by Metrnl. Gene expression in cells treated with PA or cells treated with PA plus Metrnl was analyzed by RNA sequencing, followed by gene ontology and KEGG enrichment analyses. The results showed that signaling pathways involved in the regulation of lipid accumulation were significantly enriched, including the thermogenesis and OXPHOS, which are primarily performed by mitochondria (Fig. 4*A*). Therefore, we hypothesized that Metrnl may play an important role in regulating mitochondrial function.

As expected, rMetrnl effectively attenuated the PA-induced decrease in mitochondrial membrane potential, which is an indicator of mitochondrial activity (Fig. 4*B*). PA treatment increased the percentage of fragmented mitochondria in RETCs, and Metrnl overexpression significantly inhibited PA-induced fragmentation of mitochondria (Fig. 4*C*). Conversely, the effect was exacerbated in Metrnl-knockdown RTECs (Fig. 4*D*). We further found that Metrnl overexpression or rMetrnl treatment significantly inhibited PA-induced mitochondrial fission machinery dynamin-1-like protein (Drp1) expression and remarkably restored the expression of mitofusin-1 (Mfn1) (Fig. 4*E*, Supplementary Fig. 4*A*). Notably, in vivo, rMetrnl treatment or overexpression of Metrnl attenuated Drp1 expression increase and Mfn1 expression decrease in *db/db* mice (Fig. 4*F*, Supplementary Fig. 4*B*), which were imbalanced in the mitochondrial dynamics of DKD mice (Supplementary Fig. 4*C*). Conversely, the dysregulation of mitochondrial fission and fusion were exacerbated by Metrnl knockdown of in RTECs (Fig. 4*G*). Moreover, Metrnl overexpression significantly increased the mRNA level of PGC-1α and TFAM (Supplementary Fig. 4*D*) and attenuated the PA-induced decline of the ratio of mitochondrial to nuclear DNA in RTEC cells (Supplementary Fig. 4*E*), indicating that Metrnl maintains mitochondrial dynamics and biogenesis.

In addition, we observed that rMetrnl treatment or Metrnl overexpression increased the levels of E3 ubiquitin-protein ligase Parkin (Park2) and Pink1 in the renal cortex of diabetic mice (Fig. 4*H*, Supplementary Fig. 4*F*). In vitro, Western blot analysis showed that exposure to PA markedly decreased Pink1 and Park2 expression in RTECs, and intriguingly, these effects were reversed by Metrnl overexpression (Fig. 4*I*). Conversely, Metrnl knockdown markedly diminished Pink1 and Park2 expression in RTECs treated with or without PA (Fig. 4*J*). Likewise, by using double immunostaining for MitoTracker and LC3, which are markers of mitochondria and autophagosomes, respectively, we observed increased colocalization of mitochondria and autophagosomes in Metrnl-overexpressing RTECs under PA conditions (Fig. 4*K*), although inhibiting autophagy with bafilomycin and NH_4Cl significantly reversed the decrease in LC3-II in rMetrnl-treated RTECs (Fig. 4*L*, Supplementary Fig. 4*G*), indicating that Metrnl could promote mitophagy by increasing the formation of mitophagosomes.

Because mitochondrial function is closely related to FAO, we examined the expression of FAO-pathway and OXPHOS-related genes. Transcription of the FAO-related genes PPARα, Cpt1α, Acadl, and PGC-1α, and the OXPHOS-related genes ATP5b and Ndufa10 were markedly increased in the renal cortex of rMetrnl-treated *db/db* mice (Fig. 4*O*). Notably, Metrnl overexpression reversed the decrease of ACOX1 and

Cpt1α), OXPHOS (Atp5b, Ndufa10), mitophagy/autophagy (Rab7, Pink1, and Atg7), and Metrnl in the proximal renal tubules of 40-week-old *db/db* mice in situ, which were normalized to that of GAPDH (*n* = 3/group). *E* and *F*: Representative images showing lipid deposition by Oil Red O staining (*E*) and Nile red staining (*F*) in kidney from STZ/HFD-induced diabetic mice, compared with mice fed an NCD. Scale bars: red, 100 μm; black, 50 μm; white, 50 μm. *G*: Immunofluorescence staining of perilipin-2 in kidney tissue of STZ/HFD-induced diabetic mice compared with mice fed an NCD. Scale bar: 50 μm. *H*: Representative Western blot of perilipin-2 expression in the renal cortex of 40-week-old *db/db* mice and STZ/HFD-induced diabetic mice compared with WT and NCD mice, respectively. *I* and *J*: Immunofluorescence (*I*) and IHC staining (*J*) images of perilipin-2 in human renal cortical tissues from patients with DKD (class II, *n* = 5; class III, *n* = 6; class IV, *n* = 7), compared with normal kidney poles (*n* = 5). Scale bars: red, 100 μm and white, 20 μm (*I*); red, 500 μm and black, 100 μm (*J*). *K*: Quantification of perilipin-2 expression (in *J*) in human renal cortical tissues from patients with DKD. Data are reported as mean ± SD. $^*P < 0.05$, $^{**}P < 0.01$.

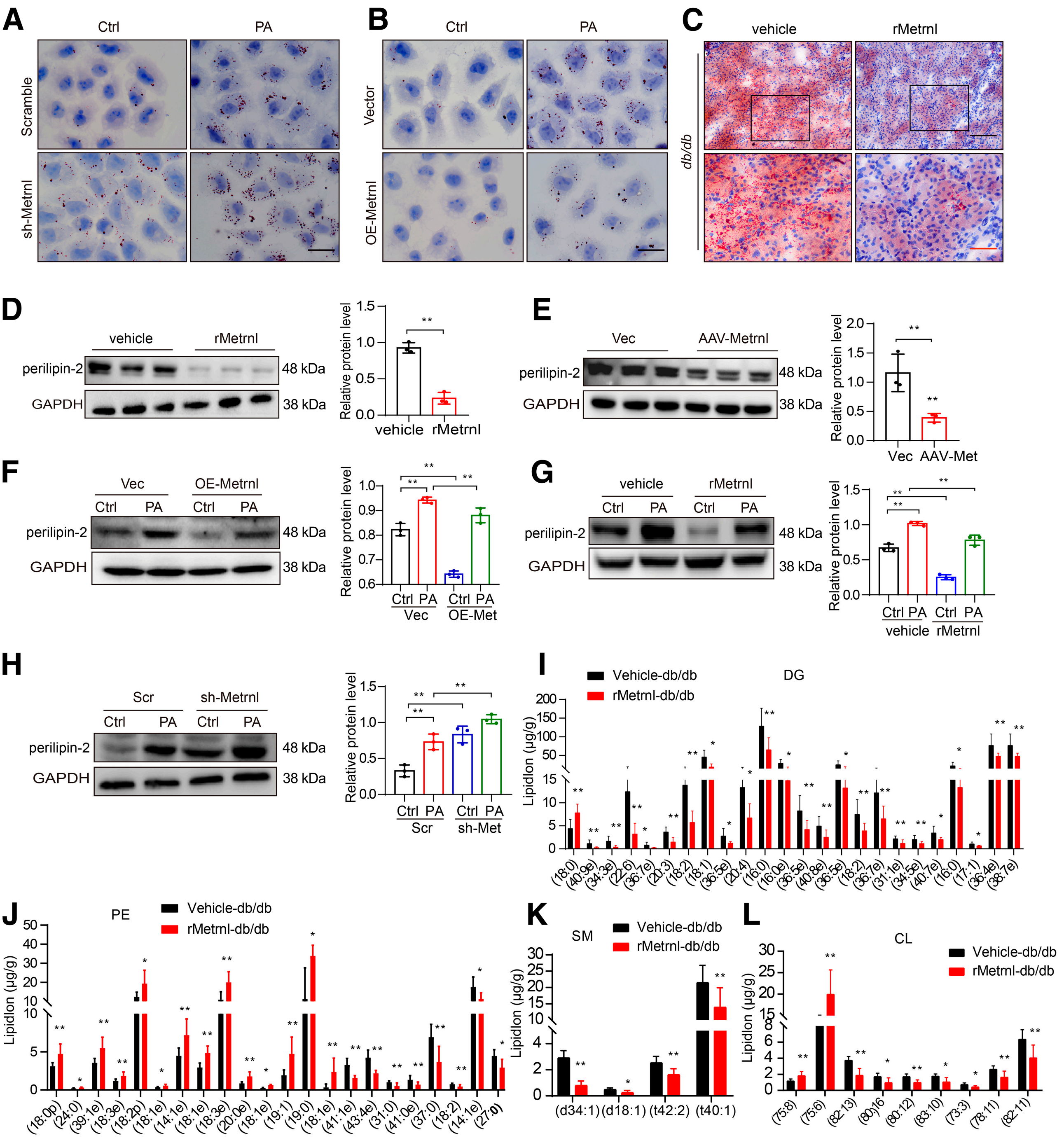

Figure 3—Metrnl negatively regulates lipid accumulation in the kidneys of mice with DKD. *A* and *B*: Representative images of Oil Red O staining in sh-Metrnl (*A*) and OE-Metrnl (*B*) stable NRK-52E cells under PA stimulation for 48 h. Scale bar: 20 μm. *C*: Representative images of Oil Red O staining of kidney in *db/db* mice treated with rMetrnl. Scale bars: black, 100 μm; red, 50 μm. *D* and *E*: Representative Western blot and quantification of perilipin-2 expression in renal cortex of *db/db* mice after rMetrnl treatment (*D*) and Metrnl overexpression (*E*) ($n = 3$ blots). *F–H*. Representative Western blot and quantification of perilipin-2 expression in OE-Metrnl (*F*) and sh-Metrnl (*H*) stable NRK-52E cells, and rMetrnl-treated NRK-52E cells (*G*) under PA stimulation for 48 h ($n = 3$ blots). *I–L*: Levels of representative individual lipid species in the kidney of *db/db* mice receiving rMetrnl treatment or control *db/db* mice ($n = 6$/group). Data are reported as mean ± SD. $^*P < 0.05$, $^{**}P < 0.01$. Ctrl, control; Vec, vector.

CPT1a expression (both are key rate-limiting enzymes that regulate FAO) (Supplementary Fig. 4*H*) and alleviated the impairment in mitochondrial respiration, as indicated by increased OCR (Fig. 4*M* and *N*) in RTECs exposed to PA, suggesting that Metrnl may activate FAO pathways and thus reduce lipid deposition. Taken together, these results suggest that Metrnl plays a key role in mitochondrial homeostasis by sustaining mitochondrial dynamics and

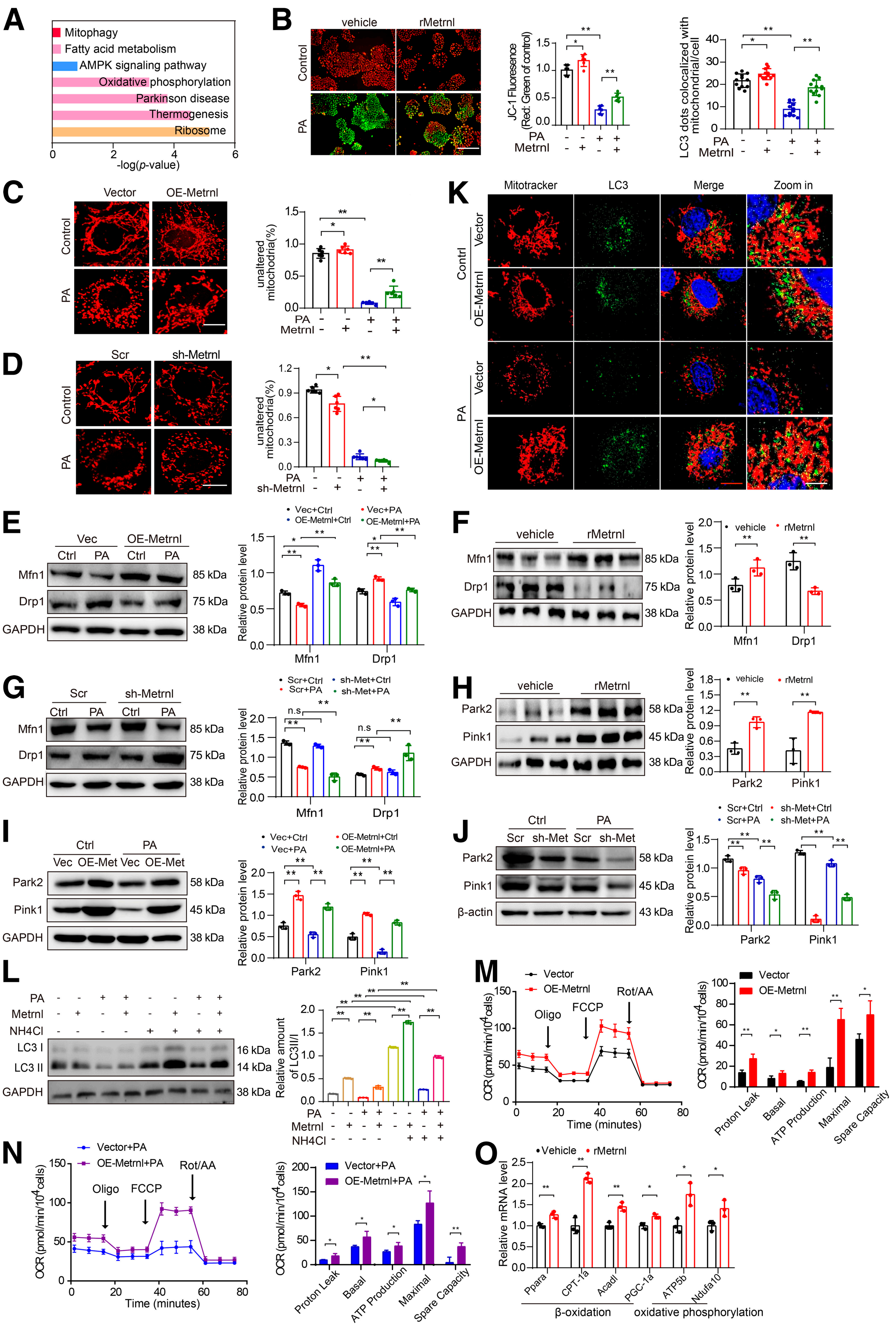

Figure 4—Changes in Metrnl expression associated with changes in mitochondrial homeostasis. *A*: Pathway enrichment analysis in PA-treated or PA-treated plus rMetrnl-cultured NRK-52E cells for 48 h, based on RNA-sequencing data (*n* = 3/group). *B*: Representative microscopic and quantification images of the mitochondrial membrane potential by JC-1 staining in NRK-52E cells after rMetrnl treatment with PA, cultured for 48 h (*n* = 6/group). Scale bar, 100 μm. *C* and *D*: Representative microscopic images and quantification of the fragmented mitochondria in Metrnl-overexpression (*C*) and Metrnl-knockdown (*D*), stable NRK-52E cells by MitoTracker (red) staining with PA, cultured for 48 h (*n* = 6/group). Scale bar, 5 μm. *E*: Representative Western blot and quantification images of the mitochondrial fission

promoting mitophagy and biogenesis in diabetic pathophysiological conditions.

Metrnl Maintains Mitochondrial Homeostasis by Upregulating Sirt3-Mediated AMPK Activity

To understand the molecular mechanism of Metrnl in mitochondrial homeostasis, we further analyzed the lipidomics data of kidneys from rMetrnl-treated *db/db* mice. Here, we focused on how SM and its accumulation may inhibit AMPK activity, which regulates mitochondrial homeostasis, optimizing OXPHOS and lipid deposition (24,28,29). The Western blot results showed that Metrnl overexpression or rMetrnl treatment induced AMPK activation (Fig. 5*A*, Supplementary Fig. 5*A*). Conversely, Metrnl knockdown prominently suppressed the activation of AMPK in RTECs exposed to PA (Fig. 5*B*). Furthermore, inhibiting AMPK expression (Supplementary Fig. 5*B*) disturbed Metrnl-mediated restoration of mitophagy, including the expression of Pink1 and Park2 (Fig. 5*C*), suggesting that Metrnl accelerated mitophagy by activating the AMPK pathway.

AMPK is a downstream target of Sirt3 that promotes lipid mobilization in adipocytes (30). In this study, we observed that Sirt3 positively regulated AMPK activation (Fig. 5*D* and *E*) in Sirt3-overexpressing or Sirt3-inhibited RTECs (Supplementary Fig. 5*C* and *D*). In addition, we analyzed the protein levels of various sirtuin members (namely, Sirt1 through Sirt7), which are important metabolic regulators (28) in response to Metrnl. The results showed that the expression of Sirt1, Sirt3, Sirt4, Sirt5, and Sirt6 was partly restored by the overexpression of Metrnl in RTECs (Fig. 5*F*).

Because Sirt3 specifically increases mitochondrial function and cellular respiration, we next focused on the potential role of Metrnl in regulating Sirt3 expression in mitochondrial homeostasis. We found that the expression of Sirt3 was significantly abated in renal biopsy samples from patients with DKD, especially from those with end-stage DKD (Fig. 5*G* and *H*), and the expression of Sirt3 was significantly positively correlated with the level of Metrnl in renal biopsy samples from patients with DKD (Fig. 5*I*). Metrnl overexpression or rMetrnl treatment visibly increased the expression of Sirt3 in RTECs (Fig. 5*A*, Supplementary Fig. 5*E*). Conversely, Metrnl deficiency inhibited Sirt3 expression in RTECs exposed to PA (Fig. 5*B*). In addition, we found that Sirt3 overexpression inhibited PA-induced Drp1 expression and remarkably restored Mfn1 expression (Supplementary Fig. 5*F*) and that these effects were reversed by Sirt3 knockdown (Supplementary Fig. 5*G*). Importantly, an inhibitor of Sirt3 abolished AMPK activation induced by Metrnl overexpression and counteracted the protective effects of Metrnl on mitochondrial dynamics in RTECs (Fig. 5*J*).

These findings suggested that Metrnl maintains mitochondrial homeostasis by upregulating the Sirt3-mediated AMPK signaling pathway, thus ameliorating lipotoxicity-induced damage in RTECs under metabolic stress.

Metrnl Promotes Thermogenesis via Sirt3-Mediated UCP1 to Alleviate Lipid Accumulation

KEGG analysis showed that the thermogenesis pathway was enriched in Metrnl-treated RTECs (Fig. 4*A*), promoting us to consider whether there was another pathway by which Metrnl reduces lipid accumulation. UCP1 is a key factor in thermogenesis and directly regulates lipid accumulation in acute kidney injury (AKI) (31), but, to our knowledge, the role of UCP1 has not been examined in DKD. Here, we found that UCP1 expression was decreased in the kidneys of DKD mice (Supplementary Fig. 6*A* and *B*), and further experiments revealed that UCP1 negatively regulated perilipin-2 expression (Fig. 6*A* and *B*) in RTECs treated with the UCP1 agonist CL316243 or by shRNA-mediated UCP1 knockdown (Supplementary Fig. 6*C* and *D*). Moreover, lipid accumulation was significantly reduced by the UCP1 agonist (Supplementary Fig. 6*E*), and exacerbated lipid accumulation was observed in UCP1-knockdown RTECs after Oil Red O staining (Supplementary Fig. 6*F*), suggesting that UCP1 regulates lipid deposition and is closely associated with DKD progression.

We found that UCP1 expression was upregulated by Metrnl overexpression (Fig. 6*C*), whereas Metrnl depletion reduced UCP1 expression in RTECs (Fig. 6*D*). Consistent with the in vitro findings, UCP1 upregulation was observed in the kidneys of rMetrnl-treated or Metrnl-

---

machinery Drp1 and Mfn1 expression in Metrnl-overexpression NRK-52E cells (n = 3 blots). *F*: Representative Western blot and quantification images of Drp1 and Mfn1 expression in renal cortex of *db/db* mice after rMetrnl treatment (n = 3 blots). *G*: Representative Western blot images and quantification of Drp1 and Mfn1 expression in Metrnl-knockdown, stable NRK-52E cells (n = 3 blots). *H*: Representative Western blot and quantification of Park2 and Pink1 expression in renal tissue of *db/db* mice after rMetrnl treatment (n = 3 blots). *I* and *J*: Representative Western blot and quantification of Park2 and Pink1 expression in Metrnl-overexpression (*I*) and Metrnl-knockdown (*J*) stable NRK-52E cells with PA, cultured for 48 h (n = 3 blots). *K*: Representative confocal microscopic images and quantification of double immunofluorescence staining for LC3 (green) and MitoTracker (red), markers for autophagosome and mitochondria individually, in Metrnl-overexpression NRK-52E cells with PA cultured for 48 h and DAPI staining for nuclei (n = 12 cells/group). Scale bars: red, 20 μm; white, 5 μm. *L*: Representative Western blot and quantification of LC3 II/I expression in Metrnl-overexpression NRK-52E cells under lysosomal acidifier NH_4Cl (25 mmol/L) stimulation for 48 h (n = 3 blots). *M* and *N*: An analysis of oxygen consumption in Metrnl-overexpression NRK-52E cells cultured with PA or not for 48 h. Those cells then were sequentially added to oligomycin (oligo) 1.5 μm), carbonyl cyanide-*p*-trifluoromethoxyphenylhydrazone (FCCP) (1.0 μm), rotenone/antimycin A (Rot/AA) (0.5 μm) to determine different parameters of mitochondrial functions according to the manufacturer's instructions (n = 3 per group). Graphical representations of proton leak OCR, basal OCR, ATP production, spare respiration capacity, and maximal OCR. *O*: Relative mRNA levels of genes related to fatty acid β-oxidation and OXPHOS in renal cortex of *db/db* mice after rMetrnl treatment (n = 3 per group). Data are reported as mean ± SD. $^*P < 0.05$, $^{**}P < 0.01$. Ctrl, control; Vec, vector.

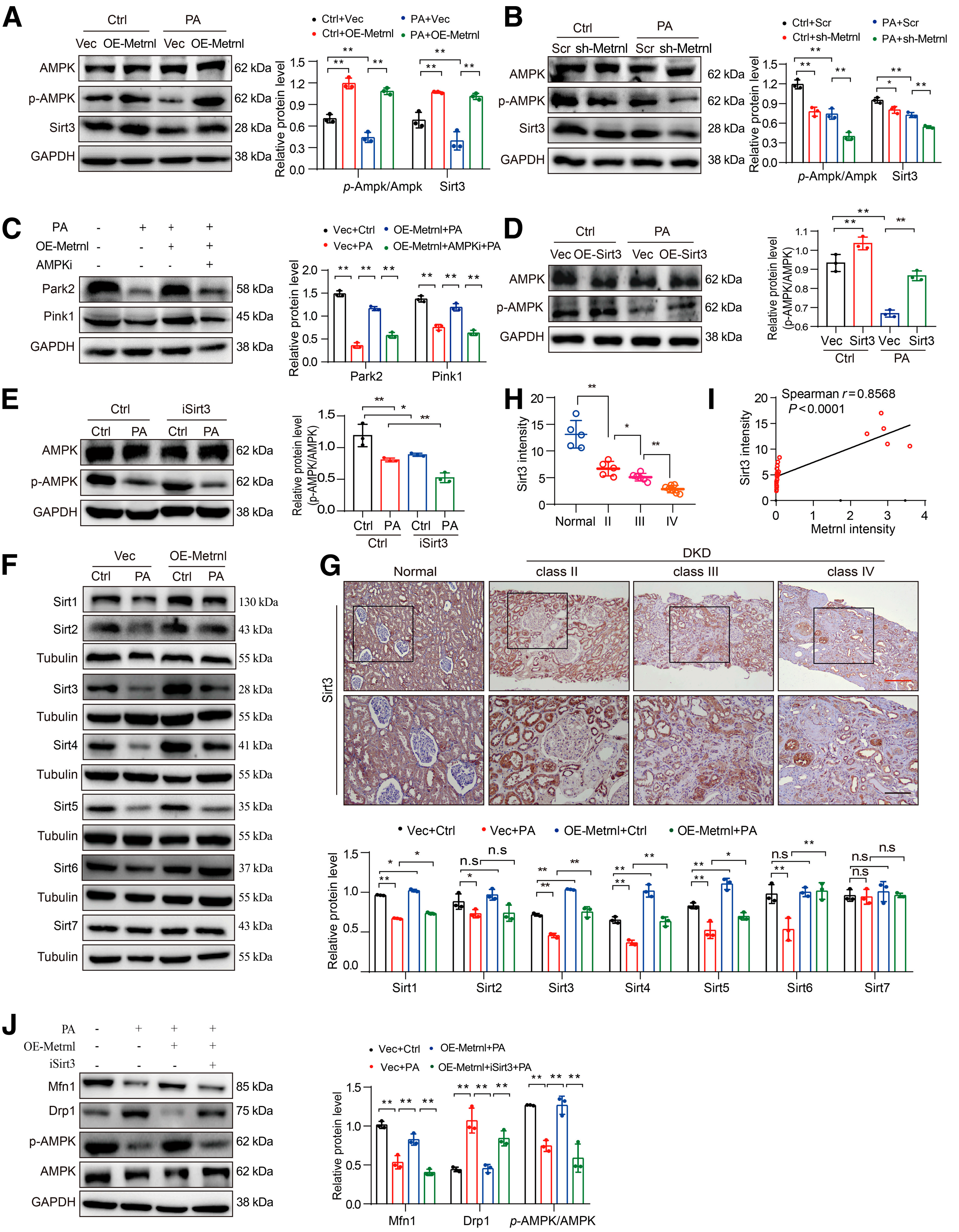

Figure 5—Metrnl maintains mitochondrial homeostasis by upregulating Sirt3-mediated AMPK activity. *A* and *B*: Representative Western blot and quantification (p-AMPK/AMPK) of the protein levels of AMPK and Sirt3 in Metrnl-overexpression (*A*) and Metrnl-knockdown (*B*) stable NRK-52E cells under PA stimulation for 48 h (*n* = 3 blots). *C*: Representative Western blot and quantification of Park2 and Pink1 expression in Metrnl overexpression, and of AMPK inhibitor (AMPKi)-treated (Dorsomorphin, 10 μmol/L) NRK-52E cells in different groups (*n* = 3 blots). *D* and *E*: Representative Western blot and quantification (p-AMPK/AMPK) of the protein levels of AMPK in Sirt3-overexpression (*D*) and Sirt3 inhibitor (iSirt3) treatment (3-TYP; 2 μmol/L) (*E*) NRK-52E cells under PA stimulation for 48 h (*n* = 3 blots). *F*: Representative

overexpressing *db/db* mice (Fig. 6*E* and *F*). Interestingly, Sirt3 overexpression obviously upregulated UCP1 and perilipin-2 expression, whereas the Sirt3 inhibitor decreased UCP1 and perilipin-2 expression in RTECs cultured with or without PA (Fig. 6*G* and *H*). Furthermore, Oil Red O staining showed that inhibiting UCP1 or Sirt3 expression in PA-treated RTECs disturbed Metrnl-mediated amelioration of lipid accumulation (Fig. 6*I*). Moreover, Sirt3 inhibition abolished Metrnl-induced UCP1 upregulation and downregulation of perilipin-2 in RTECs (Fig. 6*J*). These results indicated that Metrnl upregulates Sirt3-mediated UCP1 expression to alleviate lipid accumulation in RTECs.

Next, we focused on elucidating how Metrnl regulates the expression of Sirt3. Our in vivo results indicated that Metrnl overexpression or rMetrnl treatment significantly enhanced PGC-1α expression (Fig. 6*E* and *F*), which regulates key mitochondrial genes and is a key transcriptional coactivator of Sirt3 (29). Similar results were determined by Western blot analysis in Metrnl-overexpressing RTECs (Fig. 6*C*). Conversely, Metrnl knockdown downregulated the expression of PGC-1α in RTECs (Fig. 6*D*). Additionally, exogenous rMetrnl treatment strikingly promoted the transcriptional activation of PGC-1α and Sirt3 in the kidney tissues of *db/db* mice (Fig. 6*K*). Importantly, the ChIP–qPCR results clearly demonstrated that PGC-1α binds to the promoter region of Sirt3, and this binding was notably increased by Metrnl overexpression in RTECs (Fig. 6*L*). Taken together, these findings suggest that Metrnl regulates Sirt3 expression through the transcriptional coactivator PGC-1α and that Metrnl mediates Sirt3-UCP1 signaling to alleviate lipid accumulation by promoting thermogenesis.

Exogenous Metrnl Ameliorates Renal Injury in Mice With DKD

We tried to assess the pharmacological effect of exogenous Metrnl on DKD. Because Metrnl is a secretory protein, we chronically administered rMetrnl to *db/db* mice (Fig. 7*A* and *B*). Furthermore, we constructed an Metrnl-overexpression animal model by tail vein injection of AAV9-Metrnl (Supplementary Fig. 7*A* and *B*). The body weight gains and plasma glucose levels of *db/db* mice after fasting were decreased by rMetrnl treatment or Metrnl overexpression (Fig. 7*C* and *D*, Supplementary Fig. 7*C* and *D*). Levels of Scr, blood urea nitrogen (BUN), and urine albumin decreased in rMetrnl-treated mice or AAV9-Metrnl mice (Fig. 7*E*–*H*, Supplementary Fig. 7*E* and *F*). H-E and PAS staining revealed improvements in renal morphology and renal tubular damage, indicating a strong reduction in the degree of renal tubular damage after an increase in Metrnl (Fig. 7*I*); epithelial–mesenchymal transition (EMT)- and extracellular matrix (ECM)-related proteins in kidney tissues of *db/db* mice were reduced after rMetrnl treatment and AAV9-Metrnl expression (Fig. 7*J* and *K*). However, the level of serum insulin was increased after rMetrnl treatment, which may be associated with the protection of islets (Fig. 7*L*).

To observe the effect of overexpression in the kidney alone, we created a Metrnl-specific overexpression mouse model through intrarenal pelvic injection of AAV9-Metrnl into *db/db* mice; the Western blot analysis showed that Metrnl was mainly upregulated in the kidney but rarely upregulated in the liver, skeletal muscle, and heart tissues (Supplementary Fig. 7*G* and *H*). H-E and PAS staining revealed improvements in renal tubular damage (Supplementary Fig. 7*I*). In addition, EMT- and ECM-related proteins in kidney tissues of *db/db* mice were reduced after Metrnl-specific overexpression (Fig. 7*M*). Levels of Scr and BUN decreased in AAV9-Metrnl mice (Fig. 7*N* and *O*); however, the fasting blood glucose level was almost unchanged (Fig. 7*P*), suggesting that Metrnl overexpression in the kidney alone also has a protective effect of on kidney under DKD conditions. Therefore, Metrnl-specific overexpression in the kidney or rMetrnl can alleviate DKD progression and may be potential therapeutic candidates for chronic kidney diseases.

DISCUSSION

Proximal tubules have abundant mitochondria and tend to mainly use free fatty acids as their energy sources, which are heavily dependent on FAO for fuel (32). DKD is associated with abnormal FAO and lipid uptake, which leads to intracellular lipid deposition and kidney failure (33). We also found that patients with DKD and DKD mice have enriched lipid accumulation, especially in the renal tubule. Therefore, therapeutic strategies to address mitochondrial function and lipid deposition may be important promising treatments for DKD.

In this study, we characterized Metrnl as a renoprotective cytokine. Exogenous rMetrnl protein administration or Metrnl-specific overexpression effectively alleviated kidney damage, although the effect of rMetrnl may be linked to the changes at a distal tissue site (i.e., skeletal muscle or fat) as a consequence of lower blood glucose level or increased insulin sensitivity. From another perspective, Metrnl may be an attractive therapeutic candidate with multiple organ effect for diabetes mellitus or chronic kidney disease, which both display pathophysiology in multiple tissues and organs of body. We

Western blot and quantification of the protein levels of various sirtuin members (Sirt1 through Sirt7) in Metrnl-overexpression stable NRK-52E cells with PA cultured for 48 h ($n = 3$ blots). *G* and *H*: Representative IHC images (*G*) and quantification (*H*) of Sirt3 expression in human renal biopsy tissues from patients with DKD (class II, $n = 5$; class III, $n = 6$; class IV, $n = 7$), compared with normal kidney poles ($n = 5$). Scale bars: red, 200 μm; black, 100 μm. *I*: Correlation between Metrnl expression (Fig. 1*B*) and Sirt3 expression (*H*) in human renal cortical tissues from patients with DKD and compared with normal kidney poles in all patients ($n = 23$). *J*: Representative Western blot and quantification protein levels of p-AMPK/AMPK, the mitochondrial fission machinery Drp1 and Mfn1 in Metrnl overexpression, and Sirt3 inhibitor-treated (iSirt3, 3-TYP; 2 μmol/L) NRK-52E cells under PA stimulation for 48 h ($n = 3$ blots). Data are reported as mean ± SD. $*P < 0.05$, $**P < 0.01$. Ctrl, control; Vec, vector.

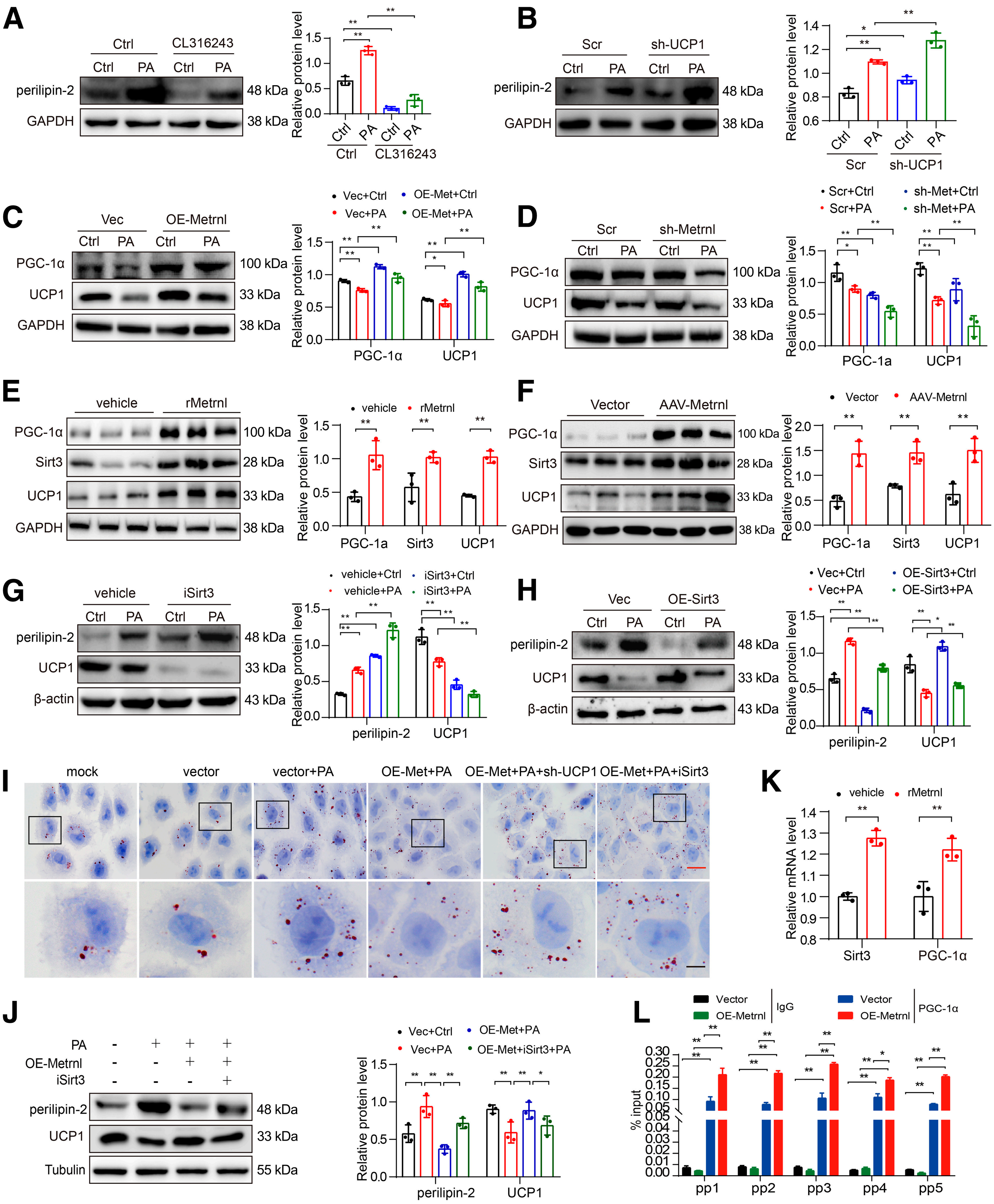

Figure 6—Metrnl promotes thermogenesis via Sirt3-mediated UCP1 to alleviate lipid accumulation. *A* and *B*: Representative Western blot and quantification of the protein levels of perilipin-2 in UCP1 agonist treatment (CL316243; 2 μmol/L) (*A*) or UCP1 knockdown (sh-UCP1) (*B*) NRK-52E cells for 48 h in different groups ($n = 3$ blots). *C* and *D*: Representative Western blot and quantification of UCP1 and PGC-1α expression in Metrnl overexpression (*C*) and Metrnl-knockdown (*D*) stable NRK-52E cells with PA cultured for 48 h ($n = 3$ blots). *E* and *F*: Representative Western blot and quantification of the protein levels of PGC-1α, UCP1, and Sirt3 in renal tissue of *db/db* mice after rMetrnl treatment (*E*) or AAV9-Metrnl overexpression (*F*) ($n = 3$ blots). *G* and *H*: Representative Western blot and quantification of the UCP1 and perilipin-2 expression in Sirt3 inhibitor (iSirt3)-treated (3-TYP; 2 μmol/L) (*G*) or Sirt3 overexpression (*H*) NRK-52E cells under PA stimulation for 48 h ($n = 3$ blots). *I*: Representative images of Oil Red O staining in UCP1-knockdown or iSirt3, with rMetrnl-treated NRK-52E cells in different groups. Scale bars: red, 20 μm; black, 5 μm. *J*: Representative Western blot and quantification of UCP1 and perilipin-2 expression in Metrnl overexpression and with iSirt3-treated (3-TYP; 2 μmol/L) NRK-52E cells under PA stimulation for 48 h ($n = 3$ blots). *K*: RT-qPCR analysis of Sirt3 and PGC-1α mRNA levels in rMetrnl-treated *db/db* mice ($n = 3$ blots). *L*: RT-qPCR analysis of Sirt3 mRNA levels with PGC-1α antibody or IgG antibody by ChIP assay in Metrnl-overexpression or control NRK-52E cells ($n = 3$). Data are reported as mean ± SD. $^*P < 0.05$, $^{**}P < 0.01$. Ctrl, control; Vec, vector.

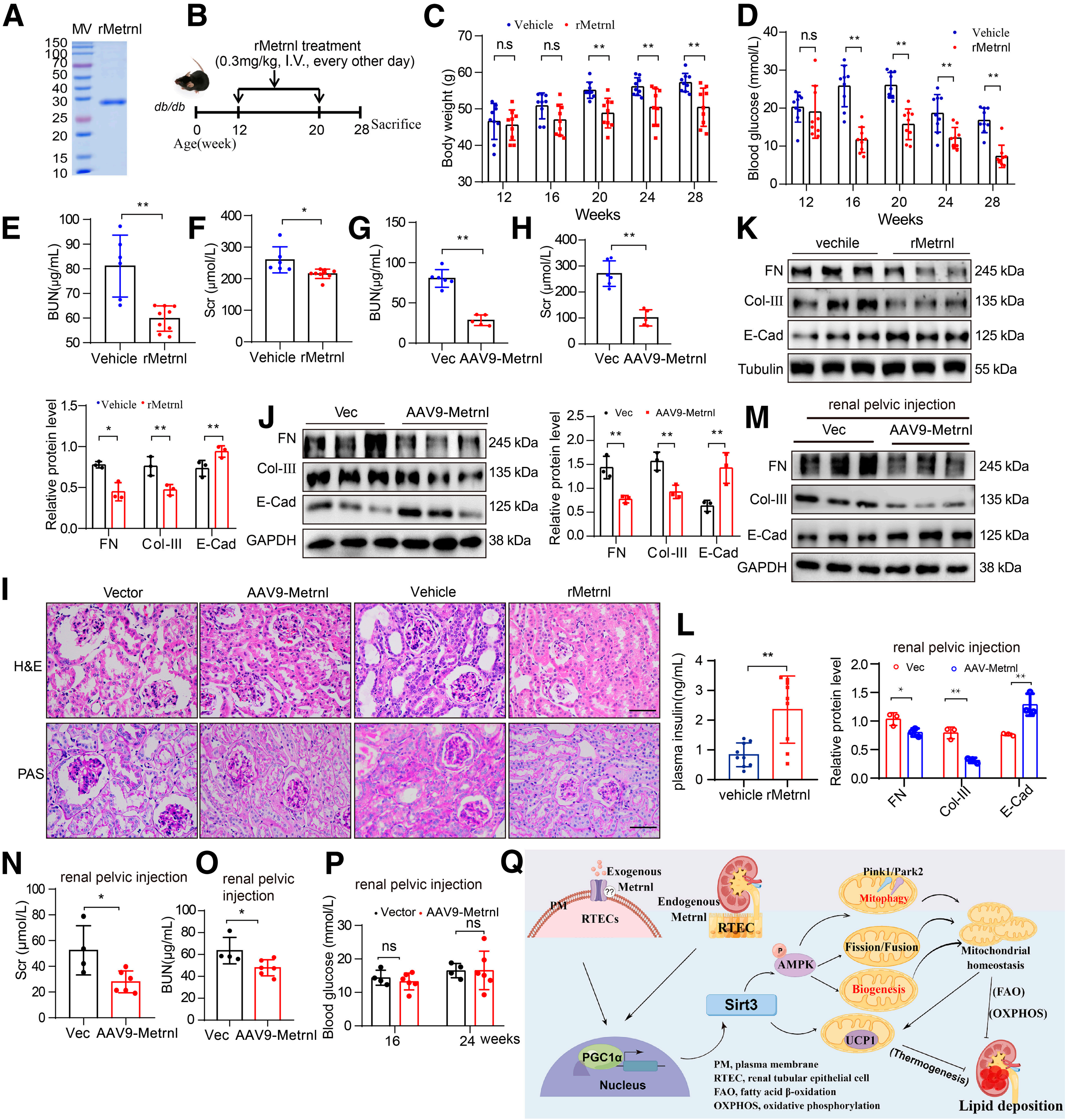

Figure 7—Exogenous Metrnl ameliorates renal injury in mice with DKD. *A* and *B*: Endotoxin removal mouse rMetrnl (*A*) and schematic of rMetrnl treatment for *db/db* mice every other day for 8 weeks (*B*). Beginning at 12 weeks of age, male *db/db* mice received tail-vein injection of rMetrnl (0.3 mg/kg body weight) or saline (vehicle) and feeding was continued until 28 weeks, when the mice were sacrificed. *C* and *D*: The body weight gains (*C*) and fasting blood glucose levels (*D*) at 12, 16, 20, 24, and 28 weeks after rMetrnl treatment (vehicle, $n = 9$; rMetrnl, $n = 9$). *E* and *F*: BUN (*E*) and Scr levels (*F*) of mice after rMetrnl treatment (vehicle, $n = 6$; rMetrnl, $n = 9$). *G* and *H*: BUN (*G*) and Scr levels (*H*) of mice treated with AAV9-Metrnl (vector, $n = 6$; AAV9-Metrnl, $n = 5$). *I*: Representative H-E and PAS staining images in *db/db* mice after rMetrnl treatment or AAV9-Metrnl virus administration. Scale bar, 50 μm. *J* and *K*: Representative Western blot and quantification of EMT- and ECM-related proteins (FN [fibronectin], collagen III [Col-III], and E-cadherin [E-Cad]) expression in renal tissue of rMetrnl-treated (*K*) and AAV9-Metrnl (*J*) mice ($n = 3$ blots). *L*: Serum insulin levels of mice after rMetrnl treatment (vehicle, $n = 9$; rMetrnl, $n = 9$). *M*: Representative Western blot and quantification of EMT- and ECM-related proteins (FN, collagen III, and E-cadherin) expression levels in kidney tissues of *db/db* mice after renal pelvic injection of AAV9-Metrnl virus ($n = 3$ blots). *N* and *O*: BUN (*N*) and Scr (*O*) levels of *db/db* mice that received renal pelvic injection of AAV9-Metrnl virus (vector, $n = 4$; AAV9-Metrnl, $n = 6$). *P*: Fasting blood glucose levels at 16 and 24 weeks of *db/db* mice after renal pelvic injection with AAV9-Metrnl virus (vector, $n = 4$; AAV9-Metrnl, $n = 6$). *Q*: A graphic model depicting the role of Metrnl in protecting the kidney from DKD pathologies by activating the PGC-1α–Sirt3–AMPK/UCP1 signaling axis. Data are reported as mean ± SD. $*P < 0.05$, $**P < 0.01$. MV, molecular weight; IV, intravenous; vec, vector.

confirmed that Metrnl was mainly expressed in renal tubules, levels of Metrnl were significantly reduced in the kidney of diabetic mice and of patients with DKD, and that Metrnl expression was significantly downregulated in response to high glucose levels or PA, suggesting that Metrnl is pathologically related to DKD. One of the most important findings was the role of Metrnl in maintaining mitochondrial homeostasis by regulating of mitophagy and mitochondrial dynamics (fission and fusion) and biogenesis. Mitochondrial fusion and fission facilitate mitochondrial quality control, and defective mitochondria are recycled via mitophagy, which removes damaged mitochondria and inhibits apoptosis (34,35). Mitophagy is regulated by a Park2/Pink1 mechanism that tags mitochondria for degradation (36). Collectively, our results elucidate a role for Metrnl in maintaining mitochondrial homeostasis in RTECs by selectively eliminating dysfunctional mitochondria through mitophagy and maintaining dynamics of mitochondria and biogenesis.

Mechanistically, we found that Sirt3 plays a pivotal role in linking Metrnl to mitochondrial homeostasis and lipid deposition. Sirt3 localizes to the mitochondrial matrix and plays an important role in regulating mitochondrial metabolism, including the tricarboxylic acid cycle, FAO, OXPHOS, and mitochondrial dynamics (37). We found Sirt3 expression was significantly reduced in the kidneys of diabetic mice and patients with biopsy-verified DKD. However, the expression of Sirt3 was markedly restored in RTECs in response to PA treatment and in mouse model of DKD with rMetrnl treatment or Metrnl overexpression. We found that Metrnl-Sirt3 signaling regulates the activity of AMPK, which plays an important role in mitophagy via a Park2/Pink1 mechanism to protect against mitochondrial dysfunction and RTEC injury in response to metabolic stress. In addition, Metrnl-Sirt3 signaling upregulates UCP1, which is located in the inner mitochondrial membrane, promotes mitochondrial inner membrane proton conduction, and decouples ATP synthesis from cellular respiration, ultimately consuming lipids to generate heat (38,39). Recently, UCP1 was shown to play a critical role in the lipid metabolism in renal clear cell carcinoma and AKI (31,40). Overall, Metrnl not only promotes lipid FAO by maintaining mitochondrial function but can directly consume lipids to promote thermogenesis through mitochondrial UCP1, thereby reducing renal lipotoxicity.

Numerous studies have established a clear link between mitochondrial health and renal resilience to AKI and chronic kidney disease (41). Key regulators of mitochondrial health, such as AMPK, sirtuins, and PGC-1α, are emerging as promising therapeutic targets (42,43). Thus, targeting the energy pathways of renal tubule cells may be beneficial for treating an array of kidney diseases, and Metrnl can target these key regulators; thus, Metrnl has promise for modulating energy metabolism to renal pharmacology. Although a recent study showed Metrnl promotes heart repair through endothelial KIT receptor tyrosine kinase (44), more research is needed to identify the cellular receptor that mediates the effects. Our observation that Metrnl induces PGC-1α in the kidney in vivo and in vitro, which, in turn, binds to the Sirt3 promoter to stimulate Sirt3 transcription, is consistent with the known role of PGC-1α as a protective factor in the kidney.

In summary, the results of our study appear to have uncovered a novel function of Metrnl, which alleviates lipid accumulation through maintaining mitochondrial homeostasis in RTECs. Mechanistically, as shown in Fig. 7Q, Metrnl not only activates Sirt3-AMPK signaling to maintain mitochondrial health and promote FAO, consequently alleviating lipid accumulation, it also directly consumes lipids to generate heat through Sirt3-UCP1. Because Metrnl is pathophysiologically related to diabetes mellitus, this work provides a new therapeutic strategy: altering Metrnl or administering Metrnl as a treatment to protect RTECs against injury in DKD.

Acknowledgments. The authors are grateful to those patients who donated their renal tissues for the studies and to the Department of Pathology, Affiliated Hospital of Guizhou Medical University, for providing the renal biopsy samples. The authors thank Molecular Machines & Industries for providing the LCM machine on trial and Dr. Yingnan Song for providing guidance of LCM technology and spatial transcriptomic analysis. The authors appreciate the help of the figure material library supported by Figdraw.

Funding. This study was supported by National Natural Science Foundation of China (grants 82000741, 32160207, 82170743, 82060111, and 8200299); China Postdoctoral Science Foundation (grant 2020M683374); Guizhou Provincial Science and Technology Projects (grant ZK [2021]402); Universities Young Science and Technology Talent Growth Project in Guizhou Province (grant KY [2021]170); and Excellent Young Talents Plan of Guizhou Medical University (grant 2021105).

Duality of Interest. No potential conflicts of interest relevant to this article were reported.

Author Contributions. Y.Z., R.Y., and B.G. conceived the idea for the project, experimental design, and the data analysis, and wrote the manuscript. Lu Liu performed Western blotting, cell imaging experiments, and analyzed data. B.J. and T.W. contributed to discussion of ideas and writing the manuscript. Y. Wu performed cell immunofluorescence experiments. L.X. performed pathological analysis. X.C. performed the immunohistochemical staining experiment. L.H. performed the LCM experiment. G.W. and Y.H. performed experiments on the animals. L.S. analyzed lipidomic data and T.Z. analyzed data from RNA sequencing. Y. Wang, Y.X., F.Z., M.S., and Lingling Liu edited the manuscript. B.G. is the guarantor of this work and, as such, had full access to all the data in the study and takes responsibility for the integrity of the data and the accuracy of the data analysis.

References

1. Du XG, Ruan XZ. Lipid metabolism disorder and renal fibrosis. Adv Exp Med Biol 2019;1165:525–541
2. Mutlu AS, Duffy J, Wang MC. Lipid metabolism and lipid signals in aging and longevity. Dev Cell 2021;56:1394–1407
3. Kume S, Uzu T, Araki S, et al. Role of altered renal lipid metabolism in the development of renal injury induced by a high-fat diet. J Am Soc Nephrol 2007;18:2715–2723
4. Stadler K, Goldberg IJ, Susztak K. The evolving understanding of the contribution of lipid metabolism to diabetic kidney disease. Curr Diab Rep 2015;15:40
5. Ducasa GM, Mitrofanova A, Fornoni A. Crosstalk between lipids and mitochondria in diabetic kidney disease. Curr Diab Rep 2019;19:144
6. Herman-Edelstein M, Scherzer P, Tobar A, Levi M, Gafter U. Altered renal lipid metabolism and renal lipid accumulation in human diabetic nephropathy. J Lipid Res 2014;55:561–572

7. Lieben L. Diabetic nephropathy: lipid toxicity drives renal disease. Nat Rev Nephrol 2017;13:194

8. Opazo-Ríos L, Mas S, Marín-Royo G, et al. Lipotoxicity and diabetic nephropathy: novel mechanistic insights and therapeutic opportunities. Int J Mol Sci 2020;21:2632

9. Miguel V, Tituaña J, Herrero JI, et al. Renal tubule Cpt1a overexpression protects from kidney fibrosis by restoring mitochondrial homeostasis. J Clin Invest 2021;131:e140695

10. Jang HS, Noh MR, Kim J, Padanilam BJ. Defective mitochondrial fatty acid oxidation and lipotoxicity in kidney diseases. Front Med (Lausanne) 2020;7:65

11. Wei PZ, Szeto CC. Mitochondrial dysfunction in diabetic kidney disease. Clin Chim Acta 2019;496:108–116

12. Galvan DL, Green NH, Danesh FR. The hallmarks of mitochondrial dysfunction in chronic kidney disease. Kidney Int 2017;92:1051–1057

13. Mishra P, Chan DC. Mitochondrial dynamics and inheritance during cell division, development and disease. Nat Rev Mol Cell Biol 2014;15:634–646

14. Szeto HH, Liu S, Soong Y, Alam N, Prusky GT, Seshan SV. Protection of mitochondria prevents high-fat diet-induced glomerulopathy and proximal tubular injury. Kidney Int 2016;90:997–1011

15. Lee JO, Byun WS, Kang MJ, et al. The myokine meteorin-like (metrnl) improves glucose tolerance in both skeletal muscle cells and mice by targeting AMPKα2. FEBS J 2020;287:2087–2104

16. Rao RR, Long JZ, White JP, et al. Meteorin-like is a hormone that regulates immune-adipose interactions to increase beige fat thermogenesis. Cell 2014;157:1279–1291

17. Miao ZW, Hu WJ, Li ZY, Miao CY. Involvement of the secreted protein Metrnl in human diseases. Acta Pharmacol Sin 2020;41:1525–1530

18. Bae JY. Aerobic exercise increases meteorin-like protein in muscle and adipose tissue of chronic high-fat diet-induced obese mice. BioMed Res Int 2018;2018:6283932

19. Chung HS, Hwang SY, Choi JH, et al. Implications of circulating Meteorin-like (Metrnl) level in human subjects with type 2 diabetes. Diabetes Res Clin Pract 2018;136:100–107

20. Wang R, Hu D, Zhao X, Hu W. Correlation of serum meteorin-like concentrations with diabetic nephropathy. Diabetes Res Clin Pract 2020;169:108443

21. Liu H, Zhou Y, Qiu H, et al. Rab26 suppresses migration and invasion of breast cancer cells through mediating autophagic degradation of phosphorylated Src. Cell Death Dis 2021;12:284

22. Zhou Y, Liu Z, Zhang S, et al. RILP restricts insulin secretion through mediating lysosomal degradation of proinsulin. Diabetes 2020;69:67–82

23. Chen J, Suo S, Tam PP, Han JJ, Peng G, Jing N. Spatial transcriptomic analysis of cryosectioned tissue samples with Geo-seq. Nat Protoc 2017;12: 566–580

24. Baek J, He C, Afshinnia F, Michailidis G, Pennathur S. Lipidomic approaches to dissect dysregulated lipid metabolism in kidney disease. Nat Rev Nephrol 2022;18:38–55

25. Wang Z, Fu W, Huo M, et al. Spatial-resolved metabolomics reveals tissue-specific metabolic reprogramming in diabetic nephropathy by using mass spectrometry imaging. Acta Pharm Sin B 2021;11:3665–3677

26. van der Veen JN, Lingrell S, da Silva RP, Jacobs RL, Vance DE. The concentration of phosphatidylethanolamine in mitochondria can modulate ATP production and glucose metabolism in mice. Diabetes 2014;63:2620–2630

27. Mitsutake S, Zama K, Yokota H, et al. Dynamic modification of sphingomyelin in lipid microdomains controls development of obesity, fatty liver, and type 2 diabetes. J Biol Chem 2011;286:28544–28555

28. Zhang J, Xiang H, Liu J, Chen Y, He RR, Liu B. Mitochondrial sirtuin 3: new emerging biological function and therapeutic target. Theranostics 2020; 10:8315–8342

29. Clark AJ, Parikh SM. Targeting energy pathways in kidney disease: the roles of sirtuins, AMPK, and PGC1α. Kidney Int 2021;99:828–840

30. Zhang T, Liu J, Tong Q, Lin L. SIRT3 acts as a positive autophagy regulator to promote lipid mobilization in adipocytes via activating AMPK. Int J Mol Sci 2020;21:372

31. Xiong W, Xiong Z, Song A, Lei C, Ye C, Zhang C. Relieving lipid accumulation through UCP1 suppresses the progression of acute kidney injury by promoting the AMPK/ULK1/autophagy pathway. Theranostics 2021;11: 4637–4654

32. Bhargava P, Schnellmann RG. Mitochondrial energetics in the kidney. Nat Rev Nephrol 2017;13:629–646

33. Kang HM, Ahn SH, Choi P, et al. Defective fatty acid oxidation in renal tubular epithelial cells has a key role in kidney fibrosis development. Nat Med 2015;21:37–46

34. Forbes JM, Thorburn DR. Mitochondrial dysfunction in diabetic kidney disease. Nat Rev Nephrol 2018;14:291–312

35. Sharma K, Karl B, Mathew AV, et al. Metabolomics reveals signature of mitochondrial dysfunction in diabetic kidney disease. J Am Soc Nephrol 2013;24:1901–1912

36. Tang C, Han H, Yan M, et al. PINK1-PRKN/PARK2 pathway of mitophagy is activated to protect against renal ischemia-reperfusion injury. Autophagy 2018;14:880–897

37. Samant SA, Zhang HJ, Hong Z, et al. SIRT3 deacetylates and activates OPA1 to regulate mitochondrial dynamics during stress. Mol Cell Biol 2014; 34:807–819

38. Golozoubova V, Hohtola E, Matthias A, Jacobsson A, Cannon B, Nedergaard J. Only UCP1 can mediate adaptive nonshivering thermogenesis in the cold. FASEB J 2001;15:2048–2050

39. Porter C. Quantification of UCP1 function in human brown adipose tissue. Adipocyte 2017;6:167–174

40. Xiao W, Xiong Z, Xiong W, et al. Melatonin/PGC1A/UCP1 promotes tumor slimming and represses tumor progression by initiating autophagy and lipid browning. J Pineal Res 2019;67:e12607

41. Zhan M, Brooks C, Liu F, Sun L, Dong Z. Mitochondrial dynamics: regulatory mechanisms and emerging role in renal pathophysiology. Kidney Int 2013;83:568–581

42. Kim J, Kundu M, Viollet B, Guan KL. AMPK and mTOR regulate autophagy through direct phosphorylation of Ulk1. Nat Cell Biol 2011;13:132–141

43. Tran MT, Zsengeller ZK, Berg AH, et al. PGC1α drives NAD biosynthesis linking oxidative metabolism to renal protection. Nature 2016;531:528–532

44. Reboll MR, Klede S, Taft MH, et al. Meteorin-like promotes heart repair through endothelial KIT receptor tyrosine kinase. Science 2022;376:1343–1347